Journal of Thermal Analysis and Calorimetry, Vol. 57 (1999) 459-472

TEMPERATURE-MODULATED CALORIMETRY OF THE CRYSTALLIZATION OF POLYMERS ANALYZED BY MEASUREMENTS AND MODEL CALCULATIONS

M. L. Di Lorenzo[1] *and B. Wunderlich*[1,2]

[1]Department of Chemistry, University of Tennessee, Knoxville, TN 37996-1600
[2]Division of Analytical and Chemical Sciences, Oak Ridge National Laboratory, Oak Ridge TN 37831-6197, USA

(Received December 10, 1998)

Abstract

The response of temperature-modulated differential scanning calorimetry (TMDSC) to irreversible crystallization of linear polymers was investigated by model calculations and compared to a number of measurements. Four different exotherms were added to a typical modulated, reversible heat-flow rate in order to simulate irreversible crystallization. It was found that the reversing heat-flow rate of the TMDSC in response to such irreversible crystallization exotherms is srongly affected by tbe shape of the transition and the phase-angle where the exotherm occurs. A comparison with the experimental data gave valuable insight into the transitions, as well as the nature of the TMDSC response which is usually limited to an analysis of the first harmonic term of the Fourier series that describes the heat-flow rate.

Keywords: crystallization, heat capacity, heat-flow rate, temperature-modulated calorimetry

Introduction

Crystallization and melting of linear macromolecules are largely irreversible processes. A small, local, reversible melting process was found for all analyzed macromolecules of sufficiently high-molar-mass as for example poly(ethylene terephthalate) [1, 2], poly(trimethylene terephthalate) [3], poly-*p*-dioxanone [4], poly(ether ether ketone) [5], and poly(oxyethylene) [6]. The fraction of the sample that undergoes reversible melting decreases with crystal perfection and, in quasi-isothermal analyses, with the time a sample resides at a given temperature in the melting region. It is assumed that the reversible melting involves local processes that occur on a sub-molecular scale. If a part of the molecule remains attached to its crystal at the time the temperature modulation reverses, the partially melted molecule can reversibly recrystallize during the cooling segment due to the remaining molecular nucleus [7, 8]. Since this process takes place at the interface between crystal and melt, it involves only a small fraction of the total material and rather precise TMDSC is necessary to quantitatively assess the process. In this paper we venture to consider

1418–2874/99/ $ 5.00

Akadémiai Kiadó, Budapest
Kluwer Academic Publishers, Dordrecht

and understand the artifacts of TMDSC that originate from the incomplete deconvolution of reversing and non reversing signals.

In the temperature region of cold-crystallization, somewhat above the glass transition, no reversibility has been observed on modulation. The supercooling is sufficiently large, so that negligible changes in crystallization rate occur during temperature modulation which typically has an amplitude of 1.0 K or less, and the melting temperature is too much higher to cause fusion in the heating segment of the modulation. The crystallization of macromolecules on cooling from the melt occurs usually also with a sufficiently large undercooling that even in the presence of crystal nuclei the temperature of the heating segment is not high enough to permit melting. In this case, however, effects of changes in crystallization rate and slow perfection of the initially grown poor ctystals may show reversible effects that are of great importance for the characterization of the crystallization and reorganization processes. In poor crystals of sufficiently low molar mass of poly(oxyethylene)s (below about 10 000 Da) it was even possible to bridge the crystallization and melting regions with the modulation amplitude [9]. Again, these are processes that need high-quality deconvolution of the TMDSC signal for their quantitative study.

The only effect seen by TMDSC during the analysis of a fully irreversible crystallization which shows no change in crystallization rate within the modulation amplitude should be a shift of the reversible heat capacity to the lower values characteristic for higher crystallinity [2, 10]. The behavior of a low-molar-mass substance is often quite different. Its crystallization and melting can be reversible as long as crystal nuclei remain on melting, and even on complete melting during the heating segment of the modulation, the inherent supercooling may be sufficiently small to be overcome during the cooling segment [11].

In order to better understand how a temperature-modulated DSC can handle irreversible crystallizations, we simulated such a process. We determined the effect of a fully irreversible crystallization exotherm on the reversing heat capacity. The combined output of the TMDSC uses the first harmonic term of the Fourier series of sample temperature and heat flow rate and involves repeated sliding averages covering as much as ±3/2 modulation cycles. Such simulations that duplicate such analyses were started several years ago in our laboratory using a simple spread-sheet program [12]. The initial calculations revealed how spikes, jumps, and sudden and gradual increases in the heat-flow rate produced small, erroneous contributions to the reversing heat capacity. Next, extensive simulations of the glass transition were performed, based on parameters gained from experimental heat-flow data from TMDSC [13, 14]. In this case it could be shown that the reversing heat-flow rate could give erroneous contributions to the non-reversing heat capacity. This was followed by simulation of reversible melting and crystallization, as found in the TMDSC of indium [11, 15]. Also, the approach to steady state in sawtooth modulations has been studied [11, 16] and will be made use of in the present work. In the current research these studies are extended by simulation of the irreversible crystallization by adding different irreversible crystallization exotherms to a sawtooth-modulated heat-flow rate and comparisons of the results with TMDSC experiments on typical polymer systems.

Experimental details

Samples of poly[imino(1-oxododecamethylene)] (nylon 12), and poly[oligo-(imino{1-oxododecamethylene})-block-oligo(oxytetramethylene)] (Pebax^{TM}) were kindly supplied by Elf-Atochem North America. The nylon 12 has a M_n of $6.0 \cdot 10^4$ Da and a M_w of $1.3 \cdot 10^5$ Da. The mass composition of the Pebax copolymer is about 20% oligo[imino(1-oxododecamethylene)] and 80% oligo(oxytetramethylene) [17]. The analyzed isotactic polypropylene (iPP) is also a commercial poduct, Shell HY 6100, with a M_w of $3.0 \cdot 10^5$ Da. The oligo(α-pinene) (PαP) used in this research is a commercial resin, Piccolyte A115^{TM} by Hercules Inc. (The Netherlands), with a M_n of 680 Da and a M_w of 1075 Da. The isotactic polypropylene/oligo(α-pinene) blends (iPP/PαP) were melt mixed according to a procedure described in [18]. The mixing ratios of iPP/PαP (in wt%) were 100/0, 90/10, 80/20, 70/30, and 50/50.

The experiments were performed with a Mettler DSC 820 (ADSC^{TM}). It represents a heat-flux calorimeter in which the modulation is governed by the sensor of the temperature of the heater and is little influenced by the evolution or absorption of latent heats due to transitions within the sample. Dry nitrogen gas with a flow rate of 20 mL min^{-1} was purged through the cell. The samples were first melted, then cooled with a sawtooth temperature program with the following characteristics: The constant, underlying cooling rate $<q>$ which is represented by the sliding average over one modulation cycle was set to 1.0 K min^{-1}, the modulation amplitude was ±1.25 K and one modulation period lasted 60 s. These parameters lead to a cooling rate of 6 K min^{-1} followed by heating at a rate of 4 K min^{-1}. Deconvolution of the underlying cooling rate and the modulation results in a pseudo-isothermal sawtooth with a rate of change of the sample temperature of ±5 K min^{-1} at the same period of 60 s and an underlying, constant cooling rate of 1 K min^{-1}.

Calculations

The calculations were carried out with a typical PC spread sheet, as described before [12], and are summarized next. A copy of the basic spread-sheet program is available from our ATHAS WWW site [19]. The experimental and simulated sample temperatures and heat-flow rates are deconvoluted into the portion arising from the underlying change and from the modulation. The oscillating portion of the signal is called the reversing portion and represented by the amplitude and, if needed, by the frequency and phase shift relative to the reference modulation. Representing the sawtooth of the sample temperature by a Fourier series, results in the following expression:

$$T_s(t) = <T_s(t)> + \sum_{\nu=1}^{\infty} [A_{Ts,\nu} \sin(\nu\omega t) + B_{Ts,\nu} \cos(\nu\omega t)] \quad (1)$$

where the underlying temperature $<T_s(t)>$ is the average over the modulation period $p(=2\pi/\omega=60$ s), and $A_{Ts,\nu}$ and $B_{Ts,\nu}$ are the amplitudes of the Fourier components ν

that must be determined in the usual manner, and ν is an integer. An analogous equation applies for the heat-flow rate $HF(t)$:

$$HF(t) = \langle HF(t)\rangle + \sum_{\nu=1}^{\infty} [A_{HF,\nu}\sin(\nu\omega t) + B_{HF,\nu}\cos(\nu\omega t)] \quad (2)$$

where $\langle HF(t)\rangle$ is the total heat-flow rate, and $A_{HF,\nu}$, and $B_{HF,\nu}$ are the corresponding amplitudes. As long as the modulation starts at t=0 and is symmetric about $\langle q\rangle t$, the modulation is centro-symmetric and all $B_{Ts,\nu}$ and $B_{HF,\nu}$ are zero, i.e., the series contain only the sinusoidal harmonics. A centro-symmetric sawtooth modulation simplifies the Fourier representation even further, it shows only odd, sinusoidal harmonics (ν=l, 3, 5, etc.). The same holds for any linear response to the sawtooth. Furthermore, representing the Fourier series by the first harmonic only, limits the series of Eqs (1) and (2) to the single amplitudes $A_{Ts}=A_{Ts,1}$ and $A_{HF}=A_{HF,1}$, respectively. It could be shown that the error caused by neglecting higher harmonics cancels when calculating heat capacities since this involves the forming of ratios of the amplitudes of A_{Ts} and A_{HF}, as can be seen below in Eq. (9), which must, however, be properly corrected for the differences in heat capacity of sample and reference calorimeters [16, 20].

The spread-sheet simulation is illustrated next for the heat-flow rate. Analogous equations hold for the sample temperature. The required integrations are replaced by summations of the simulated data, assumed to be collected at a rate of one point per s. Averaging the heat-flow rate over one modulation period p eliminates the sinusoidal component and yields the total heat-flow rate $\langle HF(t)\rangle$ of the first harmonic. Note that only the first and all even harmonics are eliminated in this procedure. The odd harmonics are not fully separated and cause a small error in the deconvolution. In the present case of collecting one data point every second, the total heat-flow rate is represented by the following average over one modulation period of 60 s [12, 16]:

$$\langle HF(t)\rangle = \frac{\sum_{t-30}^{t+30} HF(t) - 1/2HF(t-30) - 1/2HF(t+30)}{60} \quad (3)$$

Next, the heat-flow rate $HF(t)$ is corrected to the pseudo-isothermal heat-flow rate at a given temperature t by subtracting the total heat-flow rate of Eq. (3): $HF_{pseudd}(t)=HF(t)-\langle HF(t)\rangle$. The average heat-flow amplitude of this pseudo-isothermal modulation over one modulation cycle is the reversing heat-flow rate. The computation of the amplitude of the first harmonic of the reversing heat-flow rate, A_{HF}, is carried out by finding the out-of-phase and in-phase components of $HF_{pseudd}(t)$, with respect to sin ωt:

$$A_{HF}\sin(\omega t - \delta) = A_{HF}\cos\delta\sin\omega t - A_{HF}\sin\delta\cos\omega t \quad (4)$$

where δ is the phase shift of the heat-flow rate relative to ω:

$$HF_{\cos}(t) = A_{\mathrm{HF}}\sin(\omega t - \delta)\cos\omega t = HF_{\mathrm{pseudo}}\cos\omega t \tag{5}$$

$$HF_{\sin}(t) = A_{\mathrm{HF}}\sin(\omega t - \delta)\sin\omega t = HF_{\mathrm{pseudo}}\sin\omega t \tag{6}$$

This is followed by averaging (integrating) over one full period p(=60 s):

$$\langle HF_{\sin}(t)\rangle = \frac{\sum_{t-30}^{t+30} HF_{\sin}(t) - 1/2HF_{\sin}(t-30) - 1/2HF_{\sin}(t+30)}{60}$$

$$[=\langle \Delta_{\mathrm{HF}}/2)\cos\delta\rangle] \tag{7}$$

$$\langle HF_{\cos}(t)\rangle = \frac{\sum_{t-30}^{t+30} HF_{\cos}(t) - 1/2HF_{\cos}(t-30) - 1/2HF_{\cos}(t+30)}{60}$$

$$[=\langle (A_{\mathrm{HF}}/2)\sin\delta\rangle] \tag{8}$$

The two expressions in brackets represent the integrals of the central parts of Eqs (5) and (6). Because Eq. (3) can be evaluated for the first time only at a time of 30 s after the begin of the experiment or simulation, Eqs (7) and (8) can be evaluated first after 60 s. A simple vector addition of the two averages gives the average maximum amplitude of the heat-flow rate due to modulation:

$$A_{\mathrm{HF}} = 2\sqrt{\langle HF_{\sin}(t)\rangle^2 + \langle HF_{\cos}(t)\rangle^2} \tag{9}$$

The deconvolution of the temperature amplitude is analogous to that of the heat-flow rate and allows to calculate the average temperature modulation amplitude $A_{\mathrm{Ts}}=\langle A_{\mathrm{Ts}}(t)\rangle$. The reversing heat capacity can, finally, be calculated by using the just calculated reversing amplitudes or their further smoothed values [20]:

$$C_{\mathrm{p}}(t) = K' \frac{\langle A_{\mathrm{HF}}(t)\rangle}{\langle A_{\mathrm{Ts}}(t)\rangle} \frac{1}{\omega} \tag{10}$$

where K' is the calibration constant when heat capacity is derived from the heat-flow rate.

Results and discussion

The simulations of the crystallization were performed by adding four differently-shaped crystallization exoterms with an amplitude comparable to the basic, reversible heat capacity which was taken from an actual measurement in a transition-free

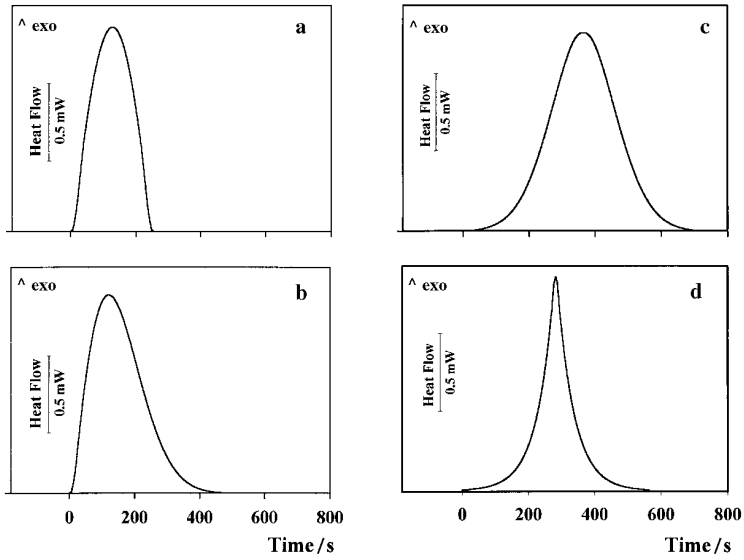

Fig. 1 Heat-flow rates corresponding to crystallization rates that were used for the simulation

temperature range. The four different crystallization curves are reported in Fig. 1. The curve 'a' is quite sharp and steep at the beginning and end of crystallization. The curve 'b', starts as steeply as curve 'a', but ends more gradually. The curve 'c' is gradual, both at the beginning and at the end of crystallization. Finally, curve 'd' starts and ends as smoothly as curve 'c', but the peak has a sharp top. The four curves simulate four types of crystallization that may be found in polymers, but the sharpness of the transition must be considered relative to the modulation period. Process (a) may be found in cold-crystallization in the presence of a large number of preformed nuclei. It begins quickly and is completed in a relatively short time as expected for fringed-micellar growth. Crystallization (b) proceeds rapidly once crystallization is initiated, but slows when crystallization nears completion as seen, perhaps, in spherulitic crystallization with termination of crystallization by impingement. Case (c) is expected if nucleation is hindered by a broad distribution of induction times. The situation (d), finally should arise if crystallization is completed rapidly relative to the modulation period, and is expected also as an instrument effect of a quick end to crystallization, followed by gradual attainment of the new steady state.

Figure 2 illustrates the experimental sawtooth-modulated heat-flow rate as measured in a transition-free region. The starting point at zero s is taken arbitrarily. The average sample temperature $<T_S>$ decreases in the direction of increasing time. Figure 2(b) shows a segment with an expanded abscissa. The first sharp increase in the heat-flow rate at 417 s occurs with a certain overshoot and represents the arpproach to steady state on cooling that is barely reached before the sawtooth modulation switches at 447 s to heating followed by another steady-state approach.

Adding now the crystallization, as shown in Fig. 1(b), starting at 495 s, 18 s after the beginning of the second cooling cycle in Fig. 2(b), results in the heat-flow rate shown in Fig. 3. Note, that it is assumed that once started, the crystallization is so far

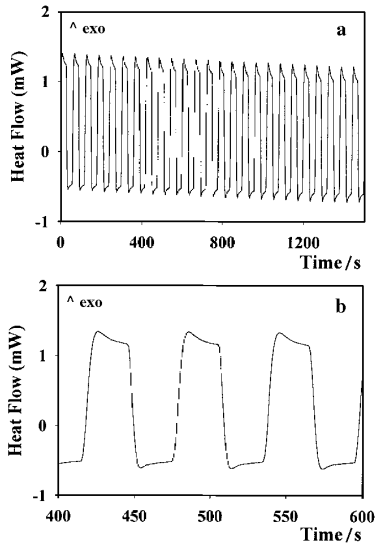

Fig. 2 The heat-flow rate $HF(t)$ in a transition-free region (a). An expansion of the time scale of (a) in the region where the crystallization was added is shown in (b). The heating cycle that starts at 477 s and ends at 506 s is used to locate the start of the irreversible crystallizations

from equilibrium that the temperature modulation does not affect the rate of crystallization.

The deconvolution of the heat-flow rate, as outlined above, yields the reversing heat capacity as reproduced in Fig. 4. Figure 4(a) shows the calculated reversing heat capacity of a crystallization that is simulated by the curve in Fig. 1(a). Sharp minima in C_p, immediately followed by smaller maxima can be linked to the beginning and end of the crystallization. Each extends for about 60 s (1.0 K). The four areas involved in the peaks are less than 0.05% of the total heat of crystallization. A small amount, but of significance if the results of TMDSC are to be used, for example, for the identification of surface melting of polymers. In Fig. 4(b) the analysis of the heat-flow rate of Fig. 3 is given which corresponds to the crystallization mode of Fig. 1(b). The first peak, linked to the initiation of the crystallization, is still present, but the gradual cessation of the crystallization yields hardly any effect. Then, Fig. 4(c) which models the gradual initiation and completion of the crystallization gives practically no contribution to the reversing heat capacity. Finally, Fig. 4(d) shows no effect in the region where the exotherm starts and ends, as in Fig. 4(c), but presents a larger discontinuity with its minimum close to the position of the maximum of the crystallization peak which occurs at about 777 s.

According to Fig. 4, the shape of the crystallization curve has a fundamental role in the incomplete separation of the irreversible latent heat from the reversible heat capacity. Although the size of the error is small, it is of importance in the possible remaining reversible processes in the crystallization and melting processes [1–9] as

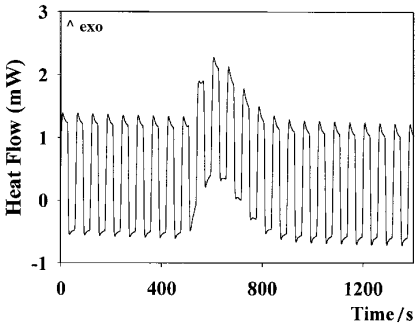

Fig. 3 Modulated heat-flow rate resulting from the addition of the irreversible crystallization of Fig. 1(b) to the heat-flow rate of Fig. 2(a)

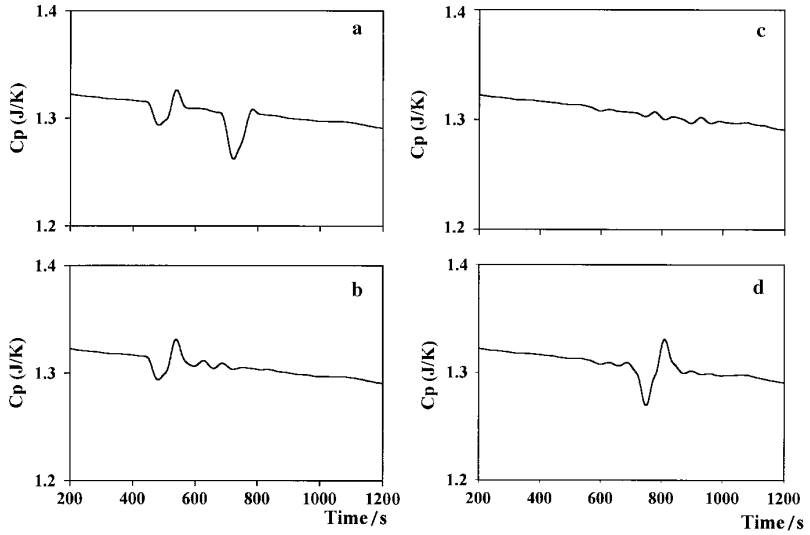

Fig. 4 Calculated reversing heat capacity using Eq. (10). Addition of the crystallization of Fig. 1, to the heat-flow rate of Fig. 2, beginning at time 595 s; (a) using Fig. 1(a); (b) using Fig. 1(b); (c) using Fig. 1(c); (d) using Fig. 1(d)

well as other latent heat effects. If the crystallization starts abruptly, as with Figs 1(a) and 1(b), the initial averages involved in the first period with crystallization decrease and produce an exotherm in the heat capacities of Figs 4(a) and (b). The reason is visible in Fig. 3. The sharp exotherm adds more to the exotherm of the first cycle than it subtracts from the endotherm. The second cycle is almost symmetric, and the gradual decrease in the subsequent cycles results in negligible imbalances. Therefore, when the crystallization starts or ends abruptly, the averages over one period cannot fully separate the irreversible portion and may produce spurious effects in the reversing heat capacity within the time interval of an irreversible transition. Similarly, a sharp maximum in the exothermic curve gives a contribution in the calcu-

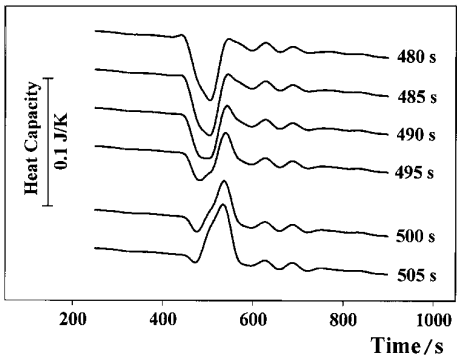

Fig. 5 Calculated reversing heat capacity using Eq. (10) for the crystallization of type 1(b), starting at the times indicated

lated reversing heat capacity in the vicinity of the peak position, as illustrated in Fig. 4(d).

Our previous attempts to simulate irreversible heat effects in TMDSC [11] involved the addition of a sudden 50% jump in the modulated heat-flow rate. It also produced a peak in $<A_{HF}>$, which, in turn, led to a small maximum in the reversing heat capacity. Conversely, a shallow exponential or even a linear drift of the heat-flow rate does not noticeably affect the reversing heat capacity. A sharp spike in the heat-flow rate of a duration of much less than one cycle could also not be compensated within the modulation period and led to a shallow minimum. The present cases are closer to actual changes in heat-flow rate expected in irreversible processes and demonstrate the importance to check the quality of the deconvolution.

In order to complete the discussion of the simulations, it remains to verify how the phase of the modulation at the starting time of the crystallization influences the calculated, reversing heat capacity. Crystallization is expected to start during a cooling segment of a modulation cycle. As before, the cooling cycle shown in Fig. 2(b) which lasts from 477 s and ends at 506 s is chosen for the start of the crystallization. Varying the initiation of the crystallization type given in Fig. 1(b) from 480 to 505 s yields the results shown in Fig. 5. The cases of Figs 1(a), (c), and (d) can easily be extrapolated from the discussion of Fig. 4.

Figure 5 illustrates that when crystallization starts at 480 s, i.e., soon after the beginning of the cooling, the calculated reversing heat capacity contains the largest exotherm. With a later start of the crystallization, the size of the exotherm decreases, and an endotherm appears and increases in magnitude with increasing delay. At about 495 s, i.e., in the middle of the cooling segment, the dimensions of the two peaks become equal in magnitude (Fig. 3). From the results of Fig. 5, it can be concluded that the presence of peaks in the reversing heat capacity during irreversible crystallization is an artifact that depends on the sharpness of the transition and the phase angle.

Finally, the simulations were compared to experiments. A number of polymers slated for analysis in our laboratory, as for instance poly(4-methylpentene-1),

poly(oxytetramethylene), and nylon 6, showed discontinuities in the reversing heat-flow rate when their crystallization was analyzed with TMDSC [21]. As an example, the reversing heat-flow rate of nylon 12 is shown in Fig. 6, together with the corresponding total heat-flow rate. From the total heat-flow rate one sees a relatively sharp beginning of crystallization, a sharp crystallization peak, and a somewhat more gradual return to steady state after crystallization. In accord with the discussion of Figs 1 to 5, this produces small discontinuities at the beginning and end of the crystallization and a larger maximum and minimum at the sharp peak. By comparison with the simulation one expects, that none of the exotherms and endotherms are true reversing effects.

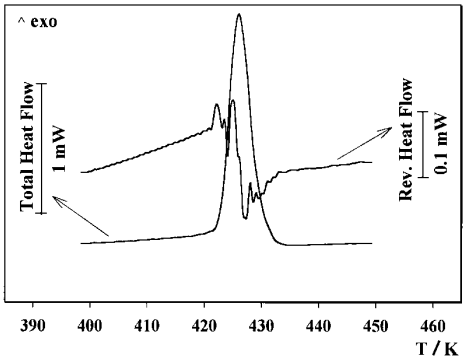

Fig. 6 Reversing heat-flow rate $HF(t)$ and total heat-flow rate $\langle HF(t) \rangle$ of nylon 12 in the crystallization rate

In multi-component systems the shape of the crystallization curve may change continuously with composition. As an example, blends produced from the crystallizable, isotactic polypropylene (iPP) and the amorphous oligomer, poly(α-pinene) (PαP) were analyzed. The crystallization behavior of iPP/PαP blends has been extensively studied and it was found that PαP slows the overall crystallization rate of iPP [17]. The total and reversing heat-flow rates of iPP/ PαP blends are shown in Fig. 7. Pure iPP (100/0 blend) crystallizes with a sharp peak and the expected artifact in the reversing heat flow. The addition of PαP retards the crystallization of iPP and shifts the overall peak to lower temperatures and broadens it. The corresponding reversing heat-flow rates were calculated with the Mettler Toledo Star^{eTM} software [22] and are displayed in Fig. 7. The discontinuities in the reversing heat-flow rate are present in the pure iPP and the blends with up to 30% PαP, but their magnitude decreases with the increasing content of PαP. The asymmetry in the reversing heat-flow rate is most likely due to a changing phase for the peak position. The bottom curve (50/50 blend) is sufficiently broad to show practically no reversing contribution (compare to Fig. 4(c)).

In the melting region of polymers some local reversibility has been observed by TMDSC. A macromolecule can partially melt during the heating portion of the modulation cycle and, if it is still attached to a crystal, it can then recrystallize on cooling. Conversely, for small molecules, crystallization and melting may be fully reversible [15]. In order to verify the absence of reversible effect on cooling in the

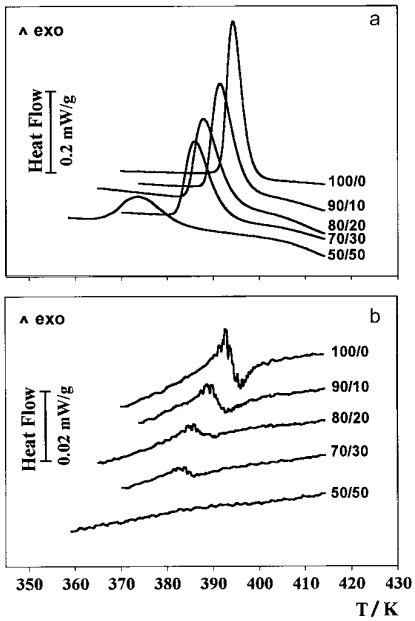

Fig. 7 Crystallization of PP/PαP blends of the indicated compositions. The upper curves are the total heat-flow rates <*HF*(*t*)> and the lower curves, the reversing heat-flow rates, *HF*(*t*)

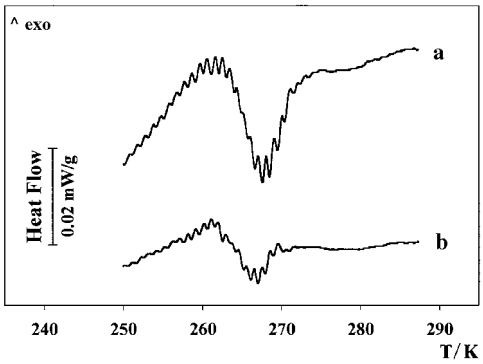

Fig. 8 The reversing heat-flow rate *HF*(*t*) of the crystallization of the oxytetramethylene segments of poly[oligo(imino{1-oxododecamethylene})-block-oligo(oxytetramethylene)] with different temperature-modulation programs. Curve (a) results for alternating cooling and heating segments as before, and curve (b) results from alternating cooling and isothermal segments

crystallization region, a temperature program that replaces the heating segments by isotherms was set up, and the results were compared with the ones obtained with the prior sawtooth with alternate cooling and heating segments. Figure 8 depicts a comparison of the reversing heat-flow rate of the multiblock copolymer with 20 oli-

goamide-12 and 80 wt% oligo(oxytetramethylene) [17] measured with both temperature programs in the temperature range where crystallization of the oligo(oxytetramethylene) blocks occurs. No large differences between the two curves can be detected, which allows to discard the hypothesis of reversible crystallization on cooling of the oxytetramethylene segments.

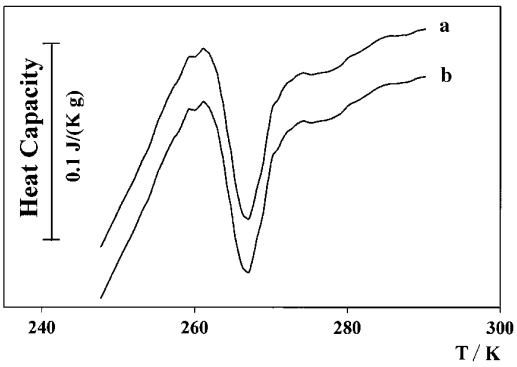

Fig. 9 Reversing heat capacity of poly[oligo(imino{1-oxododecamethylene})-block-oligo(oxytetramethylene)] calculated by accounting for (a) the first harmonic of the Fourier series of Eq. (1)(ν=1) only, and (b) the first to eleventh harmonics of the Fourier series represented in Eq. (1) (by ν=1, 3, 5, 7, 9 and 11)

Finally, the reversing heat-capacity of Eq. (10) was calculated by approximating the reversing heat-flow rate of Fig. 8(a) with the Fourier series of Eq. (1). By using only the first term of the series, the result of Fig. 9(a) was obtained. An error in the amplitude of the heat-flow rate of 19% is produced when using only the term with ν=l, but as long as the response to the modulated temperature is linear, the same deviation occurs in A_{Ts} [16] and cancels in Eq. (10). In order to improve the accuracy of the calculations, the Fourier series with terms up to ν=11 was computed and used for the generation of the curve shown in Fig. 9(b). No substantial differences between the curves (a) and (b) can be seen, as expected. The discontinuities in the reversing heat capacity are not due to the approximations used in the representation of the modulation data, but result from the deconvolution of the total and pseudo-isothermal quantities using Eq. (3).

Conclusions

The reversing response in a TMDSC experiment can be affected by an irreversible latent heat of crystallization. The reversing heat-flow rate is strongly influenced by the shape of the crystallization peak. Sharp, irreversible transitions may 1ead to the observation of peaks in the reversing part of the heat-flow rate that may be confused with small, reversible transitions.

Our simulations provide a useful tool to investigate the nature of irreversible or partially reversible transitions by comparing the experimental results with a simu-

lated curve with a shape that is similar to the total heat-flow rate exotherm. Only if the detected reversing heat-flow rate is larger than observed in the simulation, is a truly reversible contribution likely.

Since the effect on the reversing heat-flow rate is small, it is possible to check the irreversibility by a simulation that makes use of the experimental total heat-flow rate abowe the baseline which looks similar to the examples in Fig. 1. More precisely the total heat-flow rate can be obtained by standard DSC. Assuming this heat-flow rate is irreversible, it is added at different phases to a reversible, modulated heat-flow rate $HF(t)$ as shown in Fig. 3. The $HF(t)$ can be taken from a temperature range where the sample is known to have no transition effects as illustrated in Fig. 2. If the simulation results demonstrated in Fig. 5 agree with the experiment, the transition is, indeed, irreversible. If not, efforts can be made to extract the reversible contribution, such as using quasi-isothermal TMDSC for times sufficiently long to eliminate all irreversible contributions.

* * *

Supported by the Division of Materials Research, National Science Foundation, Polymers Program, number DMR-9703692, and the Division of Materials Sciences, Office of Basic Energy Sciences, U.S. Department of Energy, under contract number DE-AC05-96OR22464 with Lockheed Martin Energy Systems, Inc.

The authors warmly thank Dr. L. Judovits of Elf-Atochem North America for supplying polyamide 12 and the Pebax™ block copolymer.

One of us, M. L. D. L., wishes to thank the Italian National Research Council (C.N.R.) for supporting her reserch at the University of Tennessee.

References

1 I. Okazaki and B. Wunderlich, Macromol. Chem., Rapid Commun., 18 (1997) 313.
2 I. Okazaki and B. Wunderlich, Macromolecules, 30 (1997) 1758.
3 M. Pyda, A. Boller, J. Grebowicz, H. Chuah and B. Wunderlich, J. Polymer Sci., Part B: Polymer Phys., 36 (1998) 2499; see also Proc. 25th NATAS Conf. in McLean, Va., Sept. 7–9, R. G. Morgan ed., (1997) 87.
4 K. Ishikiriyama, M. Pyda, G. Zhang, T. Forschner, J. Grebowicz and B. Wunderlich, J. Macromol. Sci.-Phys., B37 (1997) 27.
5 A. Wurm, M. Merzlyakov and C. Schick, submitted for publication in Coll. Polym. Sci.
6 K. Ishikiriyama and B. Wunderlich, Macromolecules, 30 (1997) 4126.
7 B. Wunderlich, Disc. Farad. Soc., 68 (1979) 239.
8 B. Wunderlich and A. Mehta, J. Polym. Sci., Polymer Phys. Ed., 12 (1979) 255.
9 K. Ishikiriyama and B. Wunderlich, J. Polymer Sci., Part B, Polymer Phys., 35 (1997) 1877.
10 A. Toda, C. Tomita, T. Oda, M, Hikosaka and Y. Saruyama, Proc. 25th NATAS Conf. in McLean, Va., Sept. 7–9, R. G. Morgan ed., (1997) 645.
11 B. Wunderlich, A. Boller, I. Okazaki, K. Ishikiriyama, W. Chen, M. Pyda, J. Pak, I. Moon and R. Androsch, accepted for publication in Thermochim. Acta.
12 B. Wunderlich, J. Thermal Anal., 48 (1997) 207.
13 B. Wunderlich and I. Okazaki, J. Thermal Anal., 49 (1997) 57.
14 L. C. Thomas, A. Boller, I. Okazaki and B. Wunderlich, Thermochim. Acta, 291 (1997) 85.
15 B. Wunderlich, I. Okazaki, K. Ishikiriyama and A. Boller, Thermochim. Acta, 324 (1998) 77.; see also Proc. 25th NATAS Conf. in McLean, Va., Sept. 7–9, R. G. Morgan, ed. (1997) 49.

16 R. Androsch, I. Moon, S. Kreitmeier and B. Wunderlich, Thermochim. Acta, accepted for publication in (1999).
17 M. L. Di Lorenzo, R. Androsch, M. Pyda and B. Wunderlich, in preparation.
18 C. Silvestre, S. Cimmino, E. D'Alma, M. L. Di Lorenzo and E. Di Pace, accepted for publication in Polymer.
19 The ATHAS Web-site URL: http://web.utk.edu/~athas.
20 B. Wunderlich, Y. Jin and A. Boller, Thermochim. Acta, 238 (1994) 277.
21 M. L. Di Lorenzo and B. Wunderlich, unpublished data.
22 Mettler Toledo Star^{e} software, Version 5.0, Mettler Toledo GmbH, Analytical Sonnenbergstrasse 74, CH-8603 Schwerzenbach, Switzerland.